PROCEEDINGS A

rspa.royalsocietypublishing.org

Research

Cite this article: Hird R, Bolton MD. 2016 Migration of sodium chloride in dry porous materials. *Proc. R. Soc. A* **472**: 20150710. http://dx.doi.org/10.1098/rspa.2015.0710

Received: 16 October 2015
Accepted: 11 January 2016

Subject Areas:
civil engineering, engineering geology, materials science

Keywords:
sodium chloride, autogenous wicking, crystallization, dendrites

Author for correspondence:
Robert Hird
e-mail: rh500@cam.ac.uk

Migration of sodium chloride in dry porous materials

Robert Hird and Malcolm D. Bolton

Geotechnical and Environmental Group, Department of Engineering, University of Cambridge, Cambridge CB2 1PZ, UK

RH, 0000-0002-8485-6070

Groundwater can saturate soil above the water table within the capillary fringe associated with the pore size of the parent soil. External evaporation has been viewed as a mechanism for enhancing upward flow, potentially creating problems of salt heave beneath roads and foundations if the groundwater is saline, analogous to concerns with efflorescence in masonry. The role of internal evaporation in promoting crystallization, and especially in altering the transport process of the pore fluid, has been recognized but is only partially understood. The purpose of this paper is to examine evidence for the upward percolation of brine accompanying salt crystallization inside a porous granular material. A series of experiments are described using vertical flow columns packed with dry sand above a reservoir of saline fluid, to explore whether salt transport could take place by autogenous wicking above the initial capillary fringe. The conditions inside the columns were monitored at specific elevations with sensors measuring bulk electrical conductivity, dielectric constant and relative humidity. Dendritic salt crystallization was observed inside the sand, accompanying surface heave. Ultimately, efflorescence on the surface led to the formation of a salt crust. Some implications for the potential damage to roads and foundations in arid regions, and to masonry subject to rising damp, are discussed.

1. Introduction

The existing paradigm for the upward movement of saline groundwater focuses on the possible raising of the groundwater table due, for example, to the suppression of surface evaporation by a newly constructed road or building [1]. Of course, the capillary fringe of the parent soil is also taken into account. The matter is important in tropical regions where sodium chloride, sodium sulfate or calcium sulfate salts cause damage

THE ROYAL SOCIETY PUBLISHING

to concrete foundations, and where road pavements can be damaged by haphazard heave caused by subsurface salt crystallization. Analogous concerns affect masonry structures where salts can migrate through stonework from mortar layers, or from the foundations, causing efflorescence on exposed surfaces. Subflorescence, also known as cryptoflorescence referring to internal salt crystallization, is associated in the literature with the surface of masonry having been sealed, and it is blamed for damage due to spalling following internal crystallization [2]. The role of internal evaporation in promoting crystallization, thereby altering the transport process of the pore fluid, is poorly understood.

Capillary transport is driven by the potential pressure gradient from the source to a receding wetting front, described with a diffusion equation in terms of sorptivity involving parameters such as the permeability of the wetting material, its porosity and initial degree of saturation. The essential boundary conditions to the flow are the superficial rate of evaporation and the associated suction at the wetting front, which itself is a function of the pore size distribution, the surface tension of the fluid, and it's wetting angle on the grains. Culligan *et al.* [3] consider the one-dimensional infiltration of a liquid into dry soil, and create a mathematical model that recognizes the variability of soil permeability with the degree of saturation of the sand. Hall *et al.* [4] use a similar model for rising damp in a wall under various environmental conditions, and note that predictions of the magnitude of flow quantity should be useful in predicting damage due salt crystallization. Some advances were made in models presented by Scherer [5] of internal crystal growth during the hydration of concrete and by Le *et al.* [6], who hypothesized the wicking action of solute films through internal crystallization. However, a lack of physical evidence regarding the process of crystallization in coarse porous materials subject to the capillary uptake of saline fluid, driven by evaporation, has obstructed understanding of the consequential damage to shallow foundations and services in arid soils, and to masonry walls.

(a) Salt migration on non-porous surfaces

There is, however, a better understanding of upward salt migration on non-porous materials. If an initially dry solid is stood in a shallow tray of concentrated brine, salt will eventually begin to migrate up the side of the object, first as a translucent layer of fine crystals and later forming an outer skin of crystals in the form of dendritic outgrowths. This phenomenon was initially referred to as creep [7,8] but here it will be termed autogenous wicking. The process begins with evaporation causing the brine solution to become supersaturated, followed by the nucleation of crystals at the brine meniscus. Further crystals develop from the solute films that bound the crystals [9,10]. The repeated formation of crystals creates a fine-grained microporous medium which enhances the upward movement of solute by capillary action, thus advancing the crystallizing front in the fashion of a wick. The process was found [11] to continue while the dendrite remained connected to the brine pool, and if the relative humidity of the surrounding air remains below the point of deliquescence (DRH approx. 75% for crystals larger than 1 µm) so that evaporation can continue from the tips of the extremities of the dendrites. Figure 1 shows salt wicking up a glass stirring rod as an initial film of semi-transparent crystallites (*a*) which later develop secondary and tertiary dendritic outgrowths (*b*). In additional demonstrations we were also able to reproduce salt self-wicking within a pack of 16 mm glass beads (*c*), so something similar was expected among grains of sand.

(b) Salt migration at porous surfaces

Previous studies of salt migration in porous media have largely been confined to near-surface effects through water evaporation from drying granular media leading to efflorescence [12,13] or to near-surface subflorescence [14]. Grain size heterogeneity and changes in porosity have been found to control efflorescence textures which govern the drying kinetics of saturated porous media [15,16].

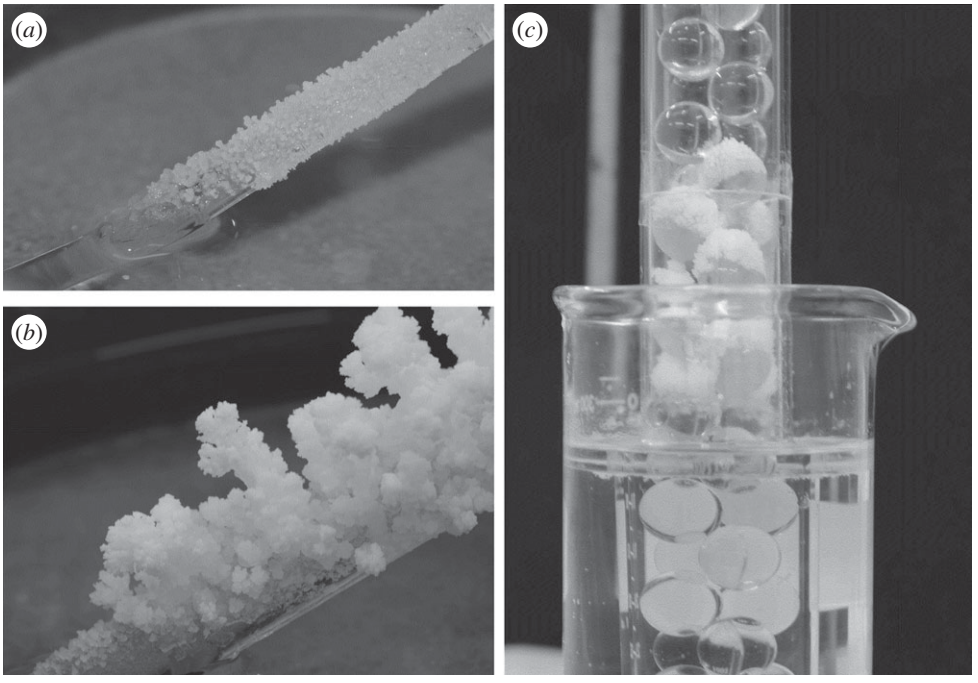

Figure 1. Salt wicking above a brine pool (*a*) covering a glass rod, (*b*) formation of dendrites, (*c*) salt precipitation on 16 mm diameter glass beads. Figure 1*b*,*c* adapted from [11].

(c) Salt migration in granular media

Broader studies of salt migration (including [17,18]) make reference to pre-wetted unsaturated soils rather than initially dry soils, so that salt transport could have been due to capillarity in the parent medium rather than self-wicking. Prior to the planning of instrumented experiments on salt transport through dry sand, an exploratory test was performed on a column of initially dry glass ballotini standing in a shallow basin of brine. Solute first migrated above the saturated capillary fringe, shown as arrow A in figure 2*a*, and then towards the surface causing subflorescence followed by efflorescence shown by arrow B. The upward path appears tree-like or dendritic (figure 2*b*,*c* [11]), resembling the shapes formed by salt on the glass rod (figure 1*b*). This observation of autogenous wicking above the saturated capillary fringe raises the question of how this mechanism modifies the conventional mechanism of capillary rise into dry media [19], what internal moisture and humidity distributions are associated with it, and when significant boundary displacements may be anticipated. The processes which led to similar dendritic structures of halite preserved in sedimentary rocks, as reported by Llewellyn [20] and Southgate [21], as well as models representing salt crystallization in masonry accompanying changes in humidity and moisture flow [22] may all have relevance here.

A variety of sensing technologies was considered.

Salt transport and the effects of crystallization, in porous sedimentary rocks, have been studied using magnetic resonance imaging and optical microscopy [23], neutron radiography and X-ray micro-tomography [24]. Salt wicking gives rise to interstitial fluid as liquid bridges between crystallites and films at crystal boundaries, and electrical conductivity measurements were able to prove connectivity between migrating salt and its source brine [11]. In porous media, the presence of salt might similarly be detected by the measurement of changes in dielectric constant and bulk electrical conductivity by time domain reflectometry (TDR) techniques. Subflorescence and efflorescence resulting from crystallization of salt can be visually observed as an increase in surface height but precise monitoring of salt crystallization in porous rock has also been

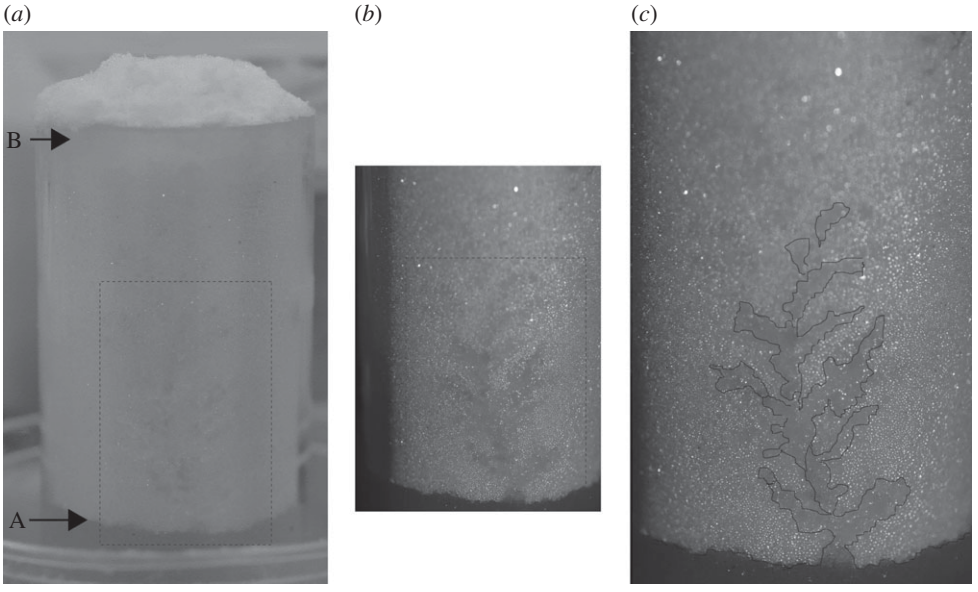

Figure 2. Dendritic migration of salt into dry glass ballotini (600–425 µm). (*a*) Showing dendrite above the capillary fringe (A) with raised surface capped by salt (B), (*b*) close-up of dendrite, (*c*) outline of dendrite accentuated.

undertaken using dilatometers [25]. The migration of salt in initially clean porous media can also be tracked through variations in relative humidity since water vapour is released at the point of salt crystallization from a fluid film [26,27]. An increase in evaporation rate within porous media has also been associated with subflorescence [14]. The points of salt crystal deliquescence and desiccation are controlled by the water vapour pressure within the pores, and the temperature, which makes relative humidity an important parameter to monitor for salt in its migratory phase and the states in which it may exist.

This paper describes a series of experiments performed in vertical flow columns packed with dry sand above a pool of saline (NaCl) fluid, to explore whether salt transport could be explained solely by the capillarity of the sand or whether additional salt wicking occurred. Extending the work of Sghaier *et al.* [14] on porous rock, it was intended to track salt rise from its source in groundwater and to link subflorescence to observations of heave. Boundary conditions were established to ensure that each test was performed in a controlled manner. These comprised constant solute concentration and a maintained elevation in the pool at the base of the column, and the exposed sand at the top of the column being subjected to a steady flow of dry air. The tests were performed in an incubator under a constant temperature of 35°C. The internal conditions were monitored at specific elevations with sensors measuring bulk electrical conductivity, dielectric constant and relative humidity.

2. Experimental techniques

(a) Materials

The groundwater used in the flow column experiments consisted of 350 g of sodium chloride reagent (Sigma Aldrich™ ≥99.8% purity) dissolved in 1 litre of deionized water. This relates to a concentration of 5.98 M where 6.2 M is the concentration of aqueous sodium chloride at saturation.

The granular medium used in the flow column was a subrounded, natural silica sand supplied by the David Ball Group Ltd (Cambridge, UK), graded as Fraction D with grain sizes between 0.40 and 0.15 mm. The particle size range chosen should sustain a saturated capillary fringe height of 63 ± 10 mm for 6 M sodium chloride brine at 35°C, as explained below. This estimate was based

upon an equivalent capillary tube using the Young–Laplace equation:

$$h_c = \frac{2T.\cos\theta}{\rho_w.g.r}, \tag{2.1}$$

where h_c is the capillary height, T is the surface tension, θ is the equilibrium or static contact angle between substrate and fluid, ρ_w is the density of the fluid, g is the acceleration due to gravity and r is the equivalent pore radius. This equivalent radius was estimated by separate capillary rise experiments in the same sand but with pure water.

The justification of values used to transform the capillary height from water to brine are based upon published data and independent tests of surface tension and contact angle. Sadeghi *et al.* [28] measured the surface tension of brine at sodium chloride concentrations up to 3 M and at temperatures between 30°C and 60°C and showed a reduction of 0.2 mN m^{-1} per 1°C which matched independent checks of surface tension using 5 M sodium chloride at 25°C and 30°C. Ozdemir *et al.* [29] measured the surface tension of 6 M brine as 81 mN m^{-1} at 20°C and so a value of 78 mN m^{-1} should be appropriate at 35°C.

Sghaier *et al.* [30] measured the static contact angle of aqueous sodium chloride at 20°C and at various concentrations by the sessile drop method on chemically cleaned glass microscope slides. The contact angle was found to increase with concentration at constant temperature. For water on treated glass plate, static contact angles were found to increase slightly with temperature [31] but specifically for sodium chloride at constant concentration but elevated temperatures, published data appear to be absent. Independent tests were therefore carried out on chemically cleaned glass plate using the Wilhemy balance method to measure the dynamic contact angle at 25°C, 30°C and 35°C in 5 M sodium chloride solution. The Wilhemy balance is an indirect force measurement of the effects of fluid on a vertically inserted glass plate. As the plate remains in contact with the fluid at constant concentration this allows better temperature control than the sessile drop method. At an insertion rate of 0.1 mm s^{-1} to a depth of 5 mm, no temperature effects were found on the advancing contact angle. This could suggest that the static contact angle of 50°, extrapolated from the data presented by Sghaier *et al.* [30], for 6 M aqueous sodium chloride could also be applied at 35°C. Laboratory analysis with a 5 M solution of sodium chloride between 25°C and 35°C showed the density of aqueous sodium chloride to reduce by 0.01 g cm^{-3} over a 15°C increment. A value of 1.182 g cm^{-3} has been taken as the density of 6 M sodium chloride at 35°C.

Water content measurements in columns of Fraction D sand which had been allowed to achieve a stable capillary rise of pure water at 20°C were obtained by weighing soil slices taken at 30 mm intervals at the end of the experiment, and by inferring water contents during the experiments from dielectric constant measurements obtained by TDR probes. The saturated capillary height of pure water was thereby estimated to be 105 mm (±15 mm). This corresponds to an equivalent pore diameter in equation (2.1) of between 0.25 and 0.33 mm. The effective pore diameter of soil is often assumed to be the diameter of particles representing the 10% fine fraction (or D_{10}) [32]. The D_{10} value for Fraction D sand based upon sieve analysis is approximately 0.20 mm, which is seen to slightly under-predict the Young–Laplace pore diameter in this case. Transforming the observed heights for water at 20°C to brine at 35°C, using the parameter values deduced from the foregoing references, the estimated height of the saturated capillary zone of brine, in the absence of evaporative internal salt crystallization, is 63 ± 10 mm. The corresponding depths of the saturated capillary fringe below the surface of the sand are given in table 1 for each experiment.

(b) Flow column

The flow columns used in the experiments were 300 mm high × 100 mm internal diameter and composed of transparent cast acrylic. A 50 mm long × 140 mm OD section of acrylic tube referred to as the 'top cap' was mounted on a stainless steel flange of the same outer diameter and an internal diameter of 100 mm. The flange was attached to the flow column by placing screws through the column walls. A clear acrylic disc of 140 mm outer diameter was attached to the top

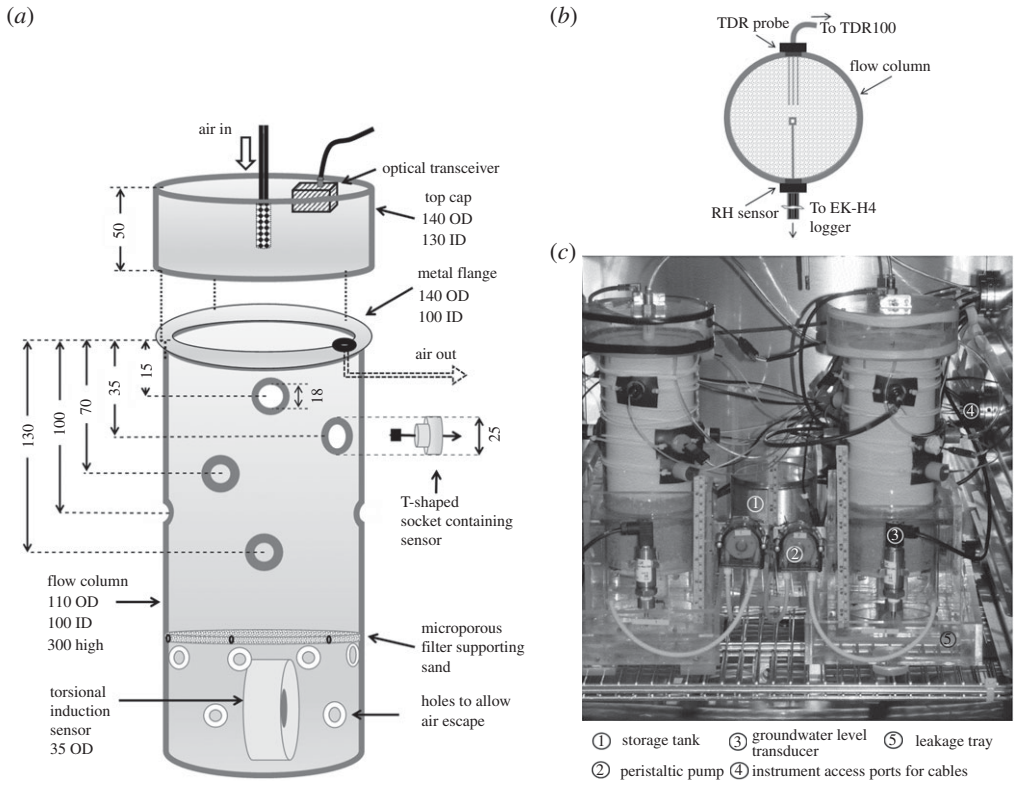

Figure 3. The flow column: (*a*) general arrangement (dimensions are given in millimetres) (not to scale); (*b*) typical plan view of sensor arrangement and (*c*) two instrumented columns within an incubator.

Table 1. Properties of each test prior to and just after adding groundwater.

experiment	dry density (g cm^{-3})	porosity (–)	Brine level (mm)[a]	estimated capillary fringe depth (mm)[a]	solute conductivity (mS cm^{-1})
1	1.70	0.36	220	157	268
2	1.68	0.37	225	162	248
3	1.68	0.37	228	165	264
4	1.71	0.35	232	169	260

[a]Below top of flow column.

of the top cap with an air diffuser placed at the centre—the diffuser would allow dry compressed air to be distributed evenly at the top of the column. An outlet for air was placed at the base of the top cap. A plastic microporous filter of 4 mm thickness and 100 mm outer diameter was placed above the base of the flow column by wall mounted support and holes drilled into the walls at and below the filter to allow air escape when the column was stood in a tray of water or solute. Sensors were sealed into 'T'-shaped sockets so that they could be mounted at the side of the column and be embedded in the sand. Holes to accommodate the sockets were cut through the flow column walls at a distance of 15, 35, 70, 100 and 130 mm from the top of the flow column, below the top cap. Each hole was 18 mm diameter with a 25 mm countersunk on the outside of the column to fit the sockets and ensure a good seal. The flow column used in the experiments is presented in figure 3.

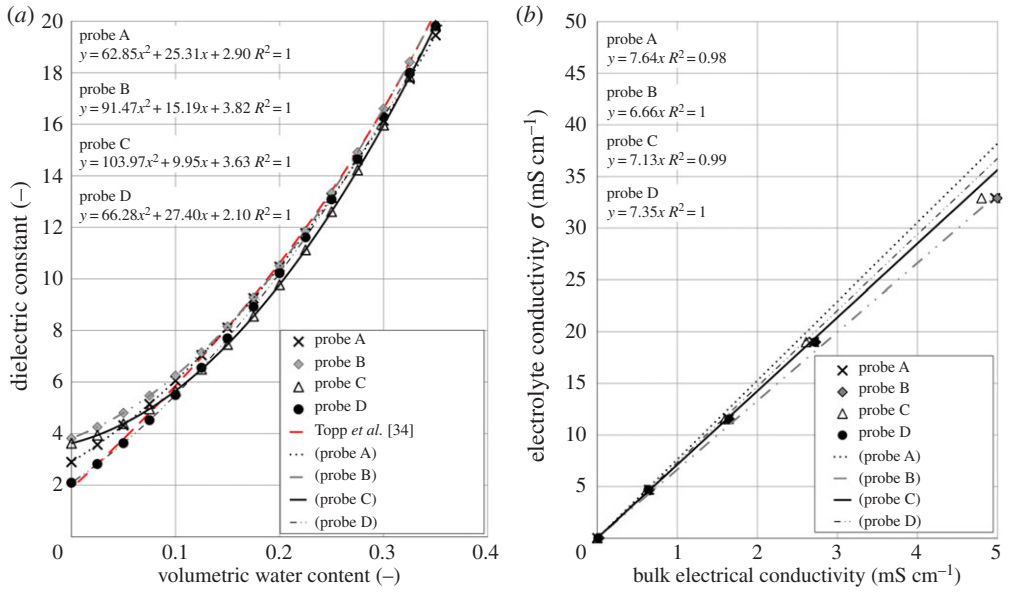

Figure 4. Calibrations for 50 mm long TDR probes: (*a*) dielectric constant versus with volumetric water content and (*b*) electrolyte electrical conductivity versus bulk electrical conductivity. (Online version in colour.)

(c) Time domain reflectometer

The presence of and change in polarizing fluids within the sand was sensed using TDR with three-rod probes. TDR is a common method for measuring changes in dielectric constant using the technique of electromagnetic wave propagation through solid metal rods acting as wave guides which are surrounded by the dielectric medium under test. The waves travel to the end of the waveguide and are reflected back. The additional delay before the electromagnetic wave returns depends upon the dielectric contrast at the end of the wave guide and this is sampled in TDR measurement. A Campbell Scientific® TDR100 was used, which combines a fast time pulse generator with a pulse length of 14 µs with a combined timed response (pulse generator and sampling circuit) of less than 300 ps. The system allows the user to select the waveform sampling resolution, which depends on the cable length and average velocity along with the length of conductor to be sampled and the signal resolution, soil properties and length of the probes. The TDR100 is connected to a multiplexer (SDMX50), also supplied by Campbell Scientific, allowing up to eight separate measurements.

Three-rod probes of 50 mm length, 1.44 mm diameter and composed of 316 grade stainless steel were fabricated according to the method described by Robinson *et al.* [33]. The probes were then calibrated to measure the offset between the changes in dielectric constant between the coaxial cable and the junction of the probes. An empirical relationship between dielectric constant and volumetric water constant was then determined using Fraction D sand compacted to a uniform porosity and saturated with deionized water before being allowed to drain naturally. Dielectric constant measurements were taken along with water loss determined by weighing, as presented in figure 4*a*, and compared with the work of Topp *et al.* [34].

TDR can also be used to measure the conductivity of the medium as the amplitude of the reflective signal is dependent on the conduction between the probes. The magnitude of the reflected signal then depends upon the concentration of ions within the pore water. This inherent property is used to measure bulk electrical conductivity in the vicinity of the probe rather than at a single point of contact (in the case of specific electrical conductivity). To correct for signal loss in the cables and across the multiplexer, the probes were calibrated according to the method

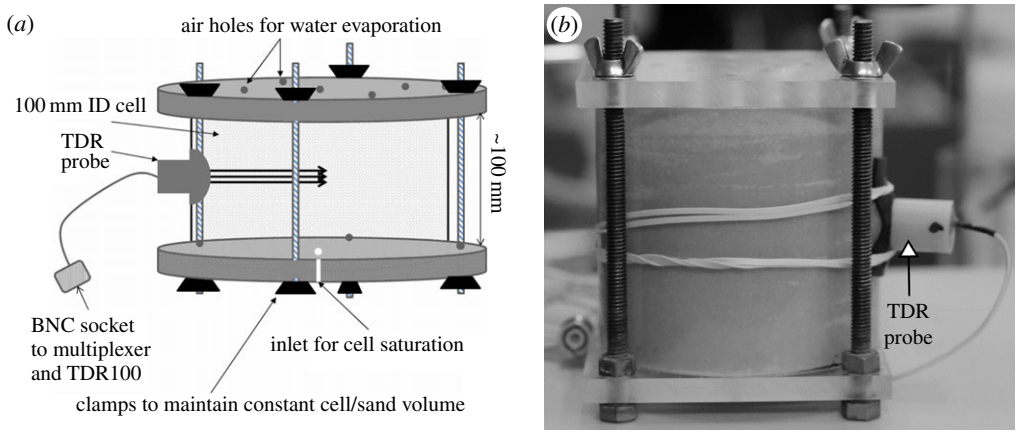

Figure 5. (*a*) Details of apparatus to measure dielectric permittivity, bulk electrical conductivity and volumetric water content; (*b*) test being carried out. (Online version in colour.)

presented by Castiglione *et al.* [35]. This involved measuring the signal reflection coefficients in open air and shorted in a brine at 284 mS cm^{-1}, to obtain the maximum and minimum conductivity respectively. The probe constant, which was unique for each probe, was obtained by immersing the probes in varying electrolyte concentrations and measuring the corresponding bulk electrical conductivity. Figure 4*b* presents the relationship between measured probe bulk electrical conductivity and conductivity of the electrolyte used to saturate the soil.

The use of TDR for measuring dielectric constant and bulk electrical conductivity has, according to the literature, been confined to soil that contains low salinity pore water. In a highly conductive medium the TDR pulse is attenuated and thus without probe and/or technique modification dielectric constant readings become unreliable [33]. However, dielectric changes can be qualitatively assessed along with bulk electrical conductivity measurements to show changes in soil in the presence of polarizing fluids.

The assessment was first performed in a test cell containing Fraction D sand compacted to a porosity of 0.35 in which a TDR probe had been horizontally placed. The cell, shown in figure 5, was saturated with electrolyte of known electrical conductivity and left to dry by evaporation. Measurements of dielectric constant and bulk electrical conductivity were periodically taken along with test cell weight to determine weight loss and average volumetric water content. Figure 6 presents the data obtained for dielectric constant and bulk electrical conductivity related to volumetric water content. The data have been limited to a dielectric constant of 20 which equates to a volumetric water content of 0.35 or full pore saturation for these soils. The empirical relationship determined by Topp *et al.* [34] shows that pore fluid up to an electrical conductivity of 22 mS cm^{-1} will also correspond to full saturation (for these probes, at this porosity). For higher salinity soils, a dielectric constant of 20 corresponds to lower volumetric water contents. There are only subtle differences of dielectric constant between levels of salinity above 22 mS cm^{-1} using the TDR method. However for bulk electrical conductivity, differences are apparent. The data shows that up to a volumetric water content of 0.08 (for dielectric constant) and 0.05 (for bulk electrical conductivity) there is a linear relationship regardless of salt concentration. For dry soils, the range of dielectric constant is three to five, but the bulk electrical conductivity is zero.

The data therefore indicate that while the dielectric constant remains below five traces of solute can provide a conductive path for bulk electrical conductivity measurements. This conductive path may be in the form of solute films between grains and within salt dendrites. These subtle differences may be used to show the presence of salt within dry media.

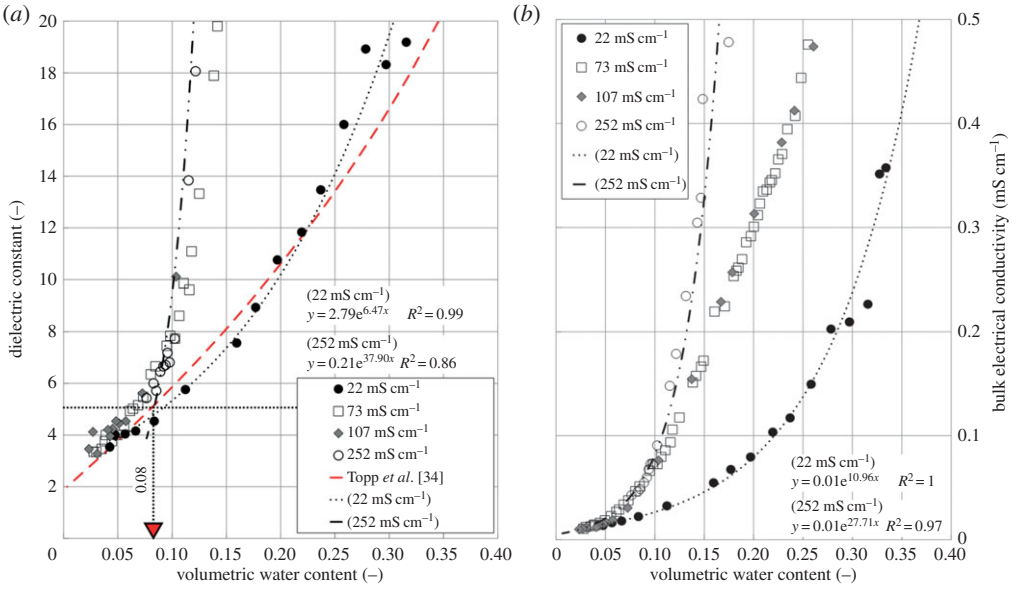

Figure 6. Dielectric constant (*a*) and bulk electrical conductivity (*b*) versus volumetric water content for pore water of elevated salinity. Horizontal dashed line in (*a*) denotes upper dielectric constant for mineral soil. (Online version in colour.)

(d) Relative humidity sensors

Relative humidity and temperature chips made by Sensirion© (SHT71) were used in the flow column experiments to measure the conditions inside the soil above the capillary fringe. The chips contain a capacitive sensor element for measuring relative humidity and a band-gap sensor for temperature measurement, both coupled to a 14 bit analogue to digital converter. The accuracy of the sensor was ±3% relative humidity. The sensors were connected to an evaluation kit (EK-H4) made by Sensirion© which included a four channel multiplexer and logger.

(e) Proximity sensor

To measure changes to the surface height at the top of the column, without contact to the surface which might alter water vapour and salt movement, a laser proximity sensor (Baumer OADM 12I6430/S35A) with a 10 mm maximum sensing range was used. Readings were made using a logging unit.

(f) Flow column preparation

To maintain boundary conditions both the depth of groundwater and the concentration of the solute had to remain constant. A torsional induction sensor (Hach Lange™) was installed in the groundwater pool below the flow column to monitor salt concentration. Both the groundwater concentration and level were maintained by injections from a separate tank of solute and administered by a peristaltic pump. Four experiments were undertaken consecutively, each with the groundwater level and concentration maintained; the properties of each flow column experiment are presented in table 1.

The sensors were placed strategically to monitor changes taking place within and above the capillary fringe and to determine the commencement of salt heave due to subflorescence and, ultimately, efflorescence at the top of the column. The sensor placement below the top of the column was as follows for all four experiments: TDR probes at 130 mm and 70 mm and relative humidity sensors at 130 mm, 100 mm and 35 mm, each measured with respect to the sand surface.

At 15 mm below the top of the column a TDR probe was inserted in experiments 1 and 4, and a relative humidity sensor in experiments 2 and 3.

To construct the flow models, dry sand was added in layers on a vibrating table around the sensors installed in the wall of the flow column. The laser proximity distance sensor (Baumer OADM 12I6430/S35A) was attached to the top cap with the laser pointing down, off-centre, onto the exposed surface of the sand. The top cap was attached to the top of the flow column and air at 1% relative humidity was allowed to flow over the top of the sand at a rate of 10 l min^{-1} and exit just below the top cap.

The brine was placed in a shallow basin, the flow column added and the experiment housed in an incubator to maintain a constant 35°C temperature.

3. Results

(a) Surface heave

Between the saturated capillary fringe where relative humidity is around the point of salt deliquescence (between 74% and 76% relative humidity) and the top of the column where the relative humidity is kept very low (about 1%), salt can precipitate within the sand. Any precipitation of salt beneath the surface may give rise to a detectable vertical movement at the surface if the salt crystallization displaces the sand rather than growing inside the pores. The salt-induced heave for each experiment is presented in figure 7. The differences between experiments can be attributed to the variability in soil properties and ground water levels shown in table 1. In experiment 1, the sensor height range was limited to allow the measurement of any negative displacement which might occur. The point where salt appears at the surface in each experiment was also recorded.

The commencement of heave and efflorescence is presented for each experiment in table 2. The data provide convenient markers to correlate with measurements from other sensors.

The first point of heave in experiment 2 at about 25 h is ignored because the rate of heave is not sustained after the initial rise. This unexplained phenomenon may be associated with anomalous salt nucleation effects and fluctuation in groundwater during initial capillary rise at the base of the column.

The flattening off of the displacement in experiments 3 and 4 from 290 h and 180 respectively is associated with changes taking place within the subflorescence zone just beneath the surface of the sand.

(b) Results within the capillary fringe

TDR probes and relative humidity sensors at 130 mm are close to the estimated capillary fringe for each experiment in table 1. The rise of fluid by capillary action above the constant solute level can be observed in figure 8 showing changes in dielectric constant and bulk electrical conductivity. The point of heave occurs well beyond the attainment of a dielectric constant of 20 in all experiments and is consequently not marked in the figure.

Relative humidity measurements at 130 mm, presented in figure 9, indirectly indicate the proximity of fluid by registering water vapour in air-filled pores. The reported ranges for deliquescence relative humidity (DRH) above which crystals absorb water vapour and pass back into solution, and the efflorescence relative humidity (ERH) at which crystals desiccate and below which continuous water films cannot be sustained, are presented on the plot as 74–77% and 41–56%, respectively [36,37], each covering a range of crystal sizes. Between these limits, salt can exist as a solid with liquid-film boundaries and can therefore form dendrites. The point of heave initiation in each experiment coincides with the point where relative humidity becomes constant within the region suitable for dendrite growth. The measured relative humidity at 100 mm depth (shown in figure 10) shows a delay in the rise of relative humidity associated with nucleation of salt above the capillary fringe.

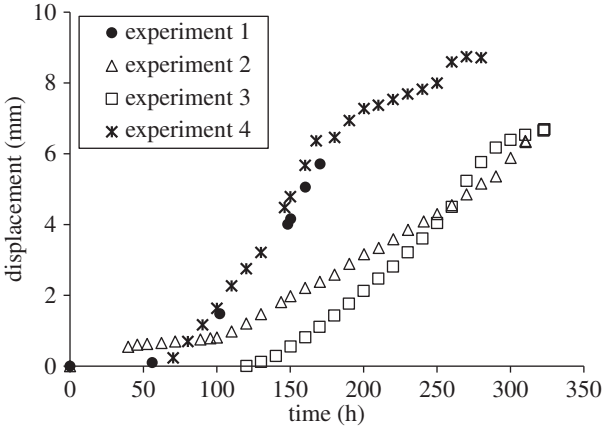

Figure 7. Surface displacement caused by salt heave.

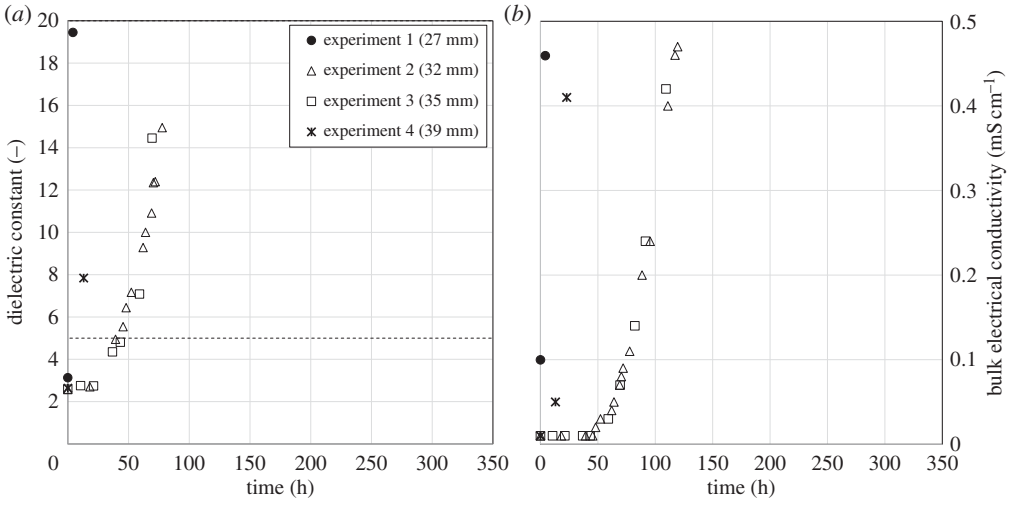

Figure 8. (*a*,*b*) Changes in dielectric constant and bulk electrical conductivity at 130 mm below the top of the flow column. Value in parenthesis is the sensor height in relation to the estimated initial height of capillary fringe.

Table 2. Time before heave and salt efflorescence to commence.

experiment	start of heave (hours)	efflorescence (hours)
1	56	97
2	102	278
3	120	326
4	53	83

(c) Results in the mid-part of the flow column

Judging simply from its colour as seen through the Perspex, rather than analysis of digital images to obtain radiance, the sand in the mid-section of the column, between 35 and 70 mm from the top of the flow column, apparently remained dry. The test data from the TDR probe at 70 mm

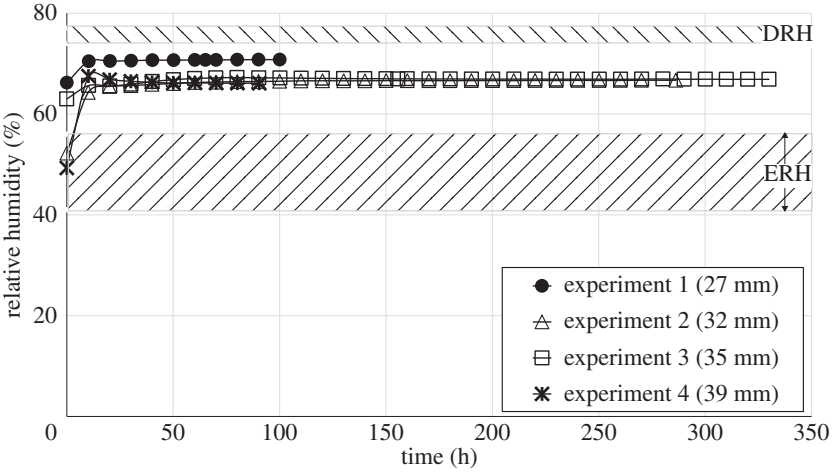

Figure 9. Change in relative humidity at 130 mm below the top of the flow column. Value in parenthesis is the sensor height in relation to the estimated initial height of capillary fringe.

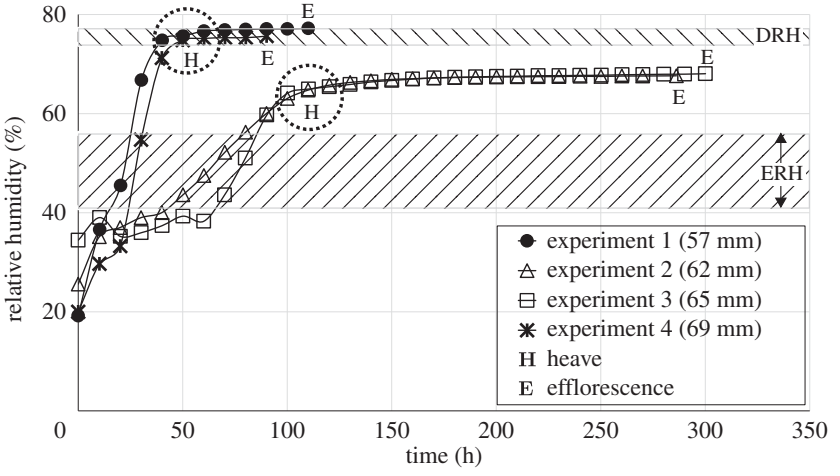

Figure 10. Change in relative humidity at 100 mm below the top of the flow column. Value in parenthesis is the sensor height in relation to the estimated initial height of capillary fringe.

are presented in figure 11. The data have been curtailed at the point where salt effloresces at the surface in each experiment. The horizontal dashed line on the dielectric constant plot represents the upper limit for mineral soil which when exceeded indicates that fluid exists within the pore space.

In tandem with table 2, the data show that up to the point of heave in each experiment the dielectric constant stays within the mineral range for soil but is slightly conductive as shown by the non-zero bulk electrical conductivity. From the point of heave to the time when salt first appeared at the surface, there is a significant increase in both bulk electrical conductivity and dielectric constant in experiments 1–3 but almost negligible change detected in experiment 4.

Relative humidity changes at 35 mm below the top of the sand are presented in figure 12. The low initial humidity is associated with the dry air stream maintained at the top of the column. The point of heave is associated with the onset of a strong increase in relative humidity although the magnitude of relative humidity at the probe differs between experiments 1 and 4, and 2

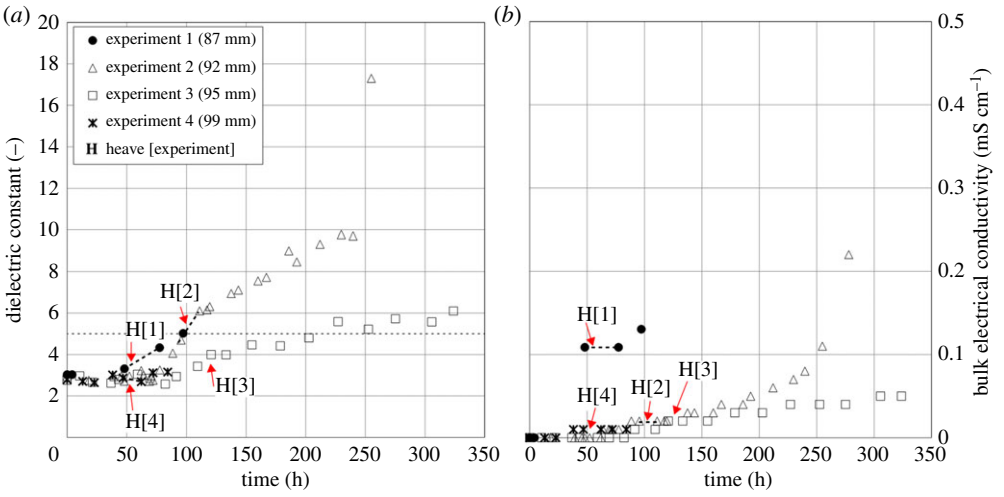

Figure 11. (*a*,*b*) Change in dielectric constant and bulk electrical conductivity at 70 mm below the top of the flow column. Value in parenthesis is the sensor height in relation to the estimated initial height of capillary fringe. (Online version in colour.)

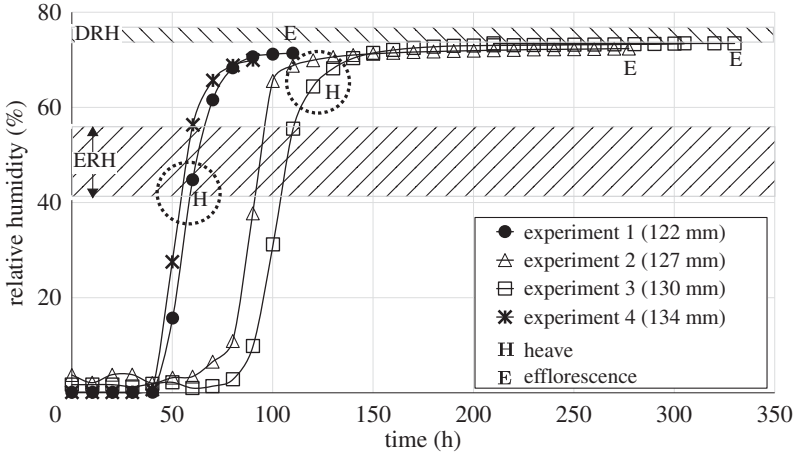

Figure 12. Change in relative humidity at 35 mm below the top of the flow column. Value in parenthesis is the sensor height in relation to the estimated initial height of capillary fringe.

and 3. In each case, the relative humidity at the onset of heave is consistent with the growth of dendrites, and the occurrence of efflorescence on the surface marks the approach of deliquescence just beneath the surface.

(d) Results close to the top of the column

Conditions in the flow column at 15 mm below the soil surface were monitored in two experiments using TDR and two experiments with relative humidity sensors. The results for dielectric constant and bulk electrical conductivity are presented in figure 13, and for relative humidity in figure 14. Dielectric constant stays within the expected range for mineral soil indicating no pore fluid. A change in bulk electrical conductivity, especially in experiment 4, may however suggest solute films are present. The relative humidity remains low up to 75 h due to the incoming dry air at the surface until just before the onset of heave when it begins to rise. During

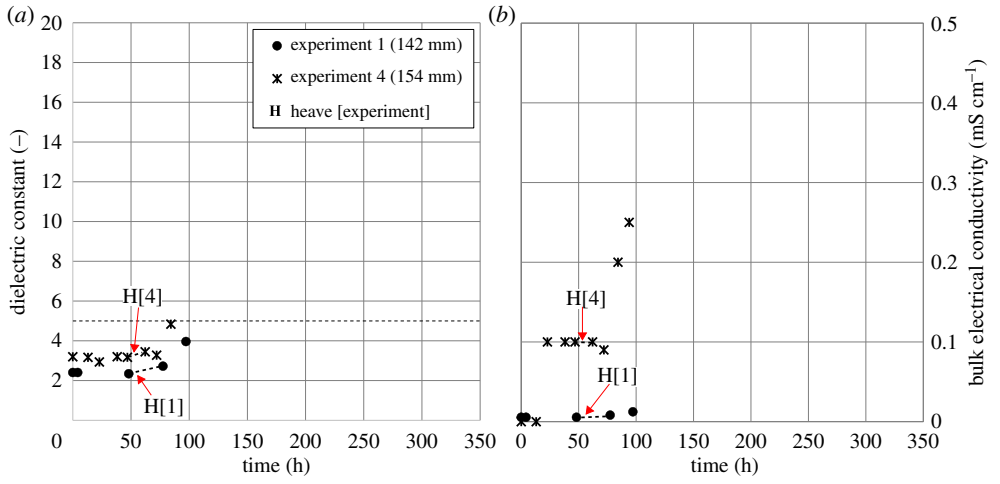

Figure 13. (*a*,*b*) Change in dielectric constant and bulk electrical conductivity at 15 mm below the top of the flow column. Value in parenthesis is the sensor height in relation to the estimated height of capillary fringe. (Online version in colour.)

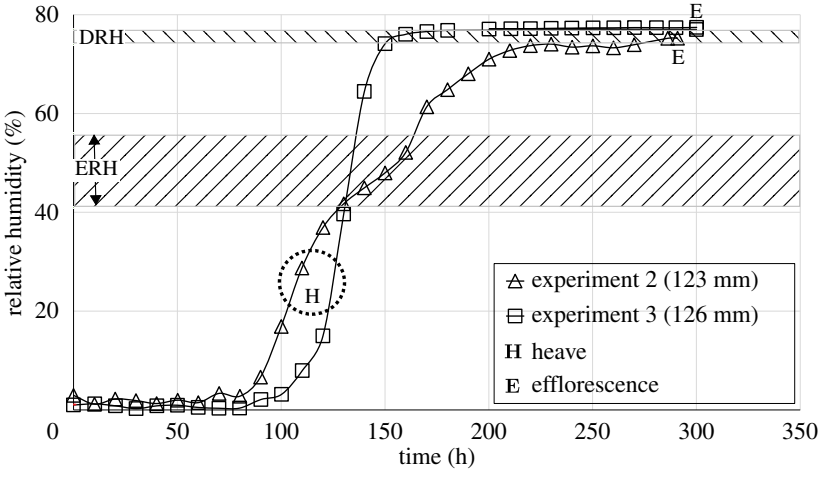

Figure 14. Change in relative humidity at 15 mm below the top of the flow column. Value in parenthesis is the sensor height in relation to the estimated initial height of capillary fringe.

heave, the relative humidity rapidly increases reaching a peak sustained humidity at around the point where salt deliquescence takes place prior to the appearance of salt at the top of the column.

4. Discussion

The rate and extent of the rise of water above the water table, into initially dry sand, is dependent on its pore size which controls both the maximum suction at the wetting front and the permeability of the sand. The initial upward migration of brine initially follows the same mechanism, albeit with different parameters corresponding to the surface tension, wetting angle and unit weight of the brine. However, an additional phenomenon then becomes apparent. Dendrites of salt crystallization begin to grow above the original capillary fringe of the parent sand. This process, described here as autogenous wicking, is controlled by the width of fluid films that coat salt crystals formed as water evaporates from the advancing dendrite. Capillarity within

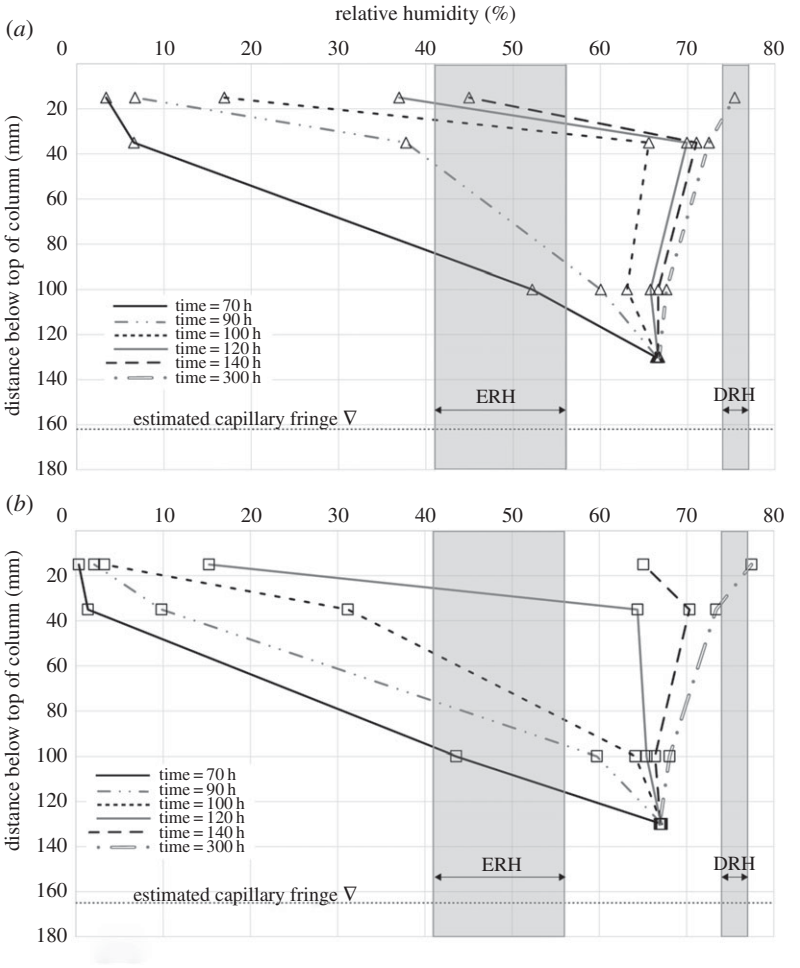

Figure 15. Relative humidity distribution as a function of sensor elevation for (*a*) experiment 2 and (*b*) experiment 3.

the dendrites should be controlled by the size of crystals more than the size of the sand. However, the exact processes which allow dendrite development are still under discussion [38]. Once a dendrite has started to grow, upward flow will continue along it in preference to the creation of independent flow paths nearby, so the advance appears as a percolation process. Similar upward dendritic growth caused by evaporation-coupled capillarity has been reported by Du *et al.* [39].

Although autogenous wicking is inherently heterogeneous, the changes in relativity humidity in the air-filled pores above the saturated capillary fringe benefit from the diffusion of water vapour, so spot values can be used to infer dendrite growth. The relative humidity around the dendrite must neither exceed the value required for salt crystals to pass back into solution by deliquescence nor be inferior to the value required to prevent desiccation of the fluid films that must connect a growing dendrite to its brine source. A delayed increase in relative humidity above the zone of capillary saturation demonstrates the advance of dendrites in the vicinity. This is shown in figure 15 where the relative humidity changes according to sensor elevation are plotted as isochrones.

Evidence of internal salt crystallization is also provided, in an integrated way, by the measurement of surface heave. Finally, salt dendrites can be exhumed from the sand above the capillary fringe at the end of an experiment which has been sufficiently long in duration to permit their growth (figure 16). Heterogeneity above the saturated zone causes the readings of other internal sensors to require a more subtle interpretation, however. TDR sensors that do not

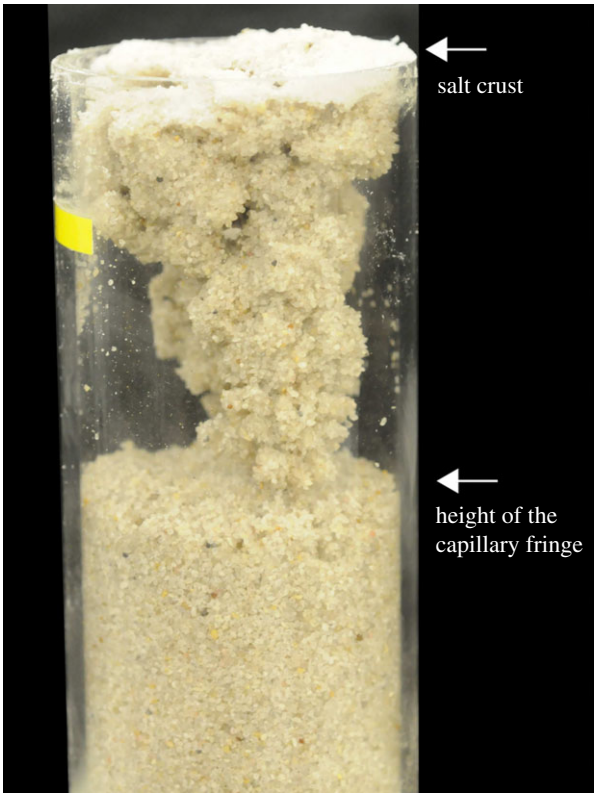

Figure 16. Relict salt dendrite within a flow column containing granular media. (Online version in colour.)

happen to intersect a dendrite may show only marginal increases in bulk electrical conductivity and dielectric constant, compared with values for dry sand.

Figure 17 presents a conceptual model of salt migration from a shallow solute reservoir through initially dry porous material until the appearance of salt at the surface. The model shows a sequence of events that could take place within the flow column as recorded by the sensors. These comprise three phases according to observable physical changes taking place in the column. The first phase, in stages (i) and (ii), establishes the capillary fringe and includes the initiation of salt dendrite growth within the existing pore structure of the sand. The second phase, in stages (iii) and (iv), features more significant subflorescence with dendrite growth sufficient to displace sand grains, and therefore promote the initiation of surface heave. In the final phase, stage (v) shows salt efflorescence taking place.

Stage (i) is captured by the TDR probes at 130 mm depth. A rapid increase in both dielectric constant and bulk electrical conductivity is consistent with the rise of the capillary fringe containing the solute, as shown in figure 8.

Stage (ii) is represented by an increase in relative humidity at 100 mm depth (shown in figure 10) in response to the general capillary rise of fluid, before stabilizing. In experiments 1 and 4, the relative humidity reaches the point of deliquescence suggesting that the solute in the capillary fringe is close to the sensor. In experiments 2 and 3, the equivalent sensor is higher than the predicted capillary fringe and relative humidity remains between the ERH and DRH upper limits. The relative humidity is maintained by water vapour release from salt dendrites above the capillary fringe. Subtle changes in dielectric constant and bulk electrical conductivity at 70 mm depth (shown in figure 11) and the slight increase in relative humidity in sensors at 35 mm depth (shown in figure 12) may indicate salt dendrite migration.

Stages (iii) and (iv) show the development of subflorescence where migrating salt dendrites encounter low relative humidity and salt crystals precipitate. Salt accumulation gives rise to

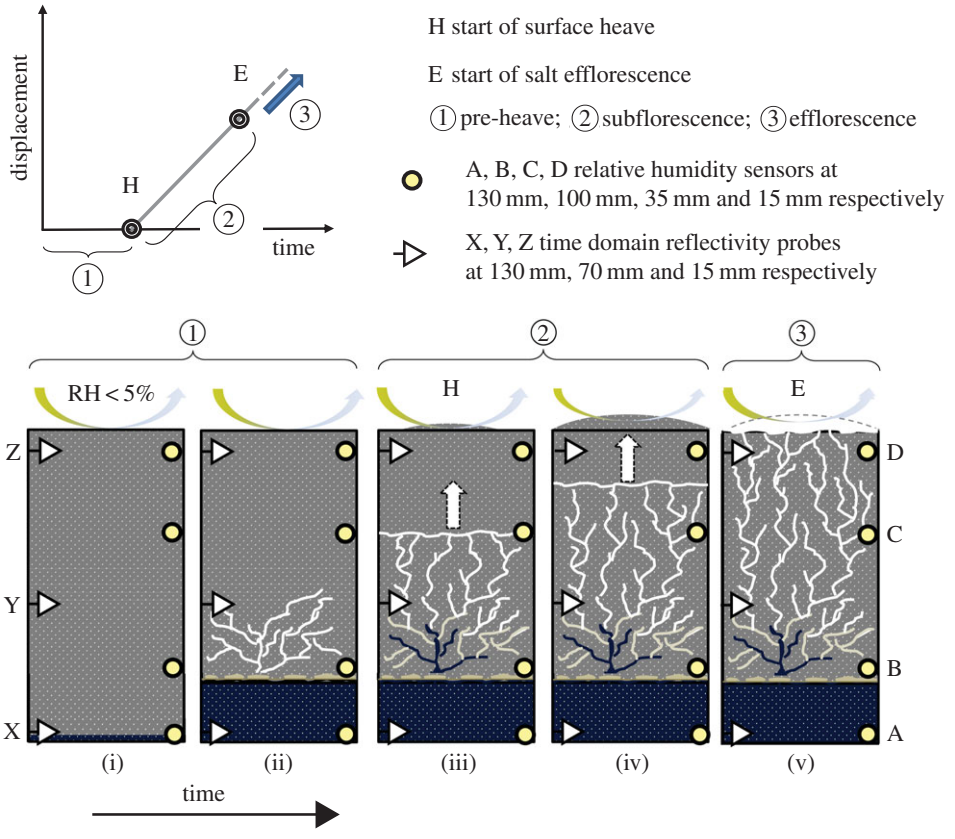

Figure 17. Conceptual model showing migration of salt through dry porous media. (Online version in colour.)

particle relocation and compaction, which is observed as surface heave as shown in figure 7. Below the zone of subflorescence the relative humidity would remain high due to the evaporation of solute from salt dendrites, shielding the region from the dry air stream at the top of the column. In experiments 1 and 4 (figure 12), the relative humidity recorded by the RH sensor at a nominal depth of 35 mm is seen to be low when heave is first detected, suggesting that subflorescence is then occurring below that elevation. By contrast, the relative humidity at first heave in experiments 2 and 3 is high at that depth indicating that subflorescence had already progressed above that sensor. In experiments 2 and 3 at the higher elevation, 15 mm below the top of the column, the relative humidity at the point of heave is low suggesting that the zone of subflorescence has not yet reached that sensor (figure 14).

Stage (v) sees dendrites arriving at the top of the column and creating efflorescence in the form of a salt crust. Relative humidity readings 15 mm below the top of the column (shown in figure 14) indicate that the point of efflorescence in the dry air is marked by deliquescence being reached immediately beneath, implying the availability of free brine below the salt crust. TDR measurements following the start of heave (figure 13) show slight increases in both dielectric constant and bulk electrical conductivity though data are confined to experiments 1 and 4 where no relative humidity measurements were made at this elevation.

5. Conclusion

Rising salt encrustation has previously been observed on non-porous surfaces in contact with a pool of brine. The mechanism has been termed autogenous wicking, and it depends on

the nucleation of salt crystals that engender capillary rise, while the solute evaporates from the growing tips of the resulting dendrites. This paper now reports evidence for a similar percolation mechanism occurring inside an initially dry granular material, above the capillary zone that could otherwise be anticipated from knowledge of its effective pore size. The new transport mechanism was examined in flow column experiments on dry sand, using sensors to monitor the changing properties of the medium as enhanced capillary rise took place and salt crystallization occurred. Changes in dielectric constant and bulk electrical conductivity showed the rise and extent of the solute in the saturated capillary fringe. Measured changes in relative humidity above the capillary fringe, coupled with surface heave, were consistent with the growth of salt dendrites above the saturated fringe, causing progressive expansion due to the internal crystallization. Subtle changes in dielectric constant and bulk electrical conductivity from probes above the saturated capillary fringe suggested that continuous solute films are present between grains boundaries in the dendrites, rather than as pore fluid within the parent sand. The ultimate evolution from the growth of internal dendrites (subflorescence) to the formation of a salt crust (efflorescence) was also recorded by the sensors. The study casts doubt on the long-term efficacy of tipping coarse, dry granular material over brine-rich soils in an attempt to prevent salt rising into road pavements or foundations placed above. Similarly, the use of coarse-grained masonry on exposed surfaces may not be an antidote to subflorescence and spalling in an environment with saline groundwater and a dry atmosphere. In each case, an impermeable membrane may be required, though further research is needed to establish appropriate conditions.

Data accessibility. The material supporting this article has been uploaded as part of the electronic supplementary material.

Authors' contributions. The experimental work, analysis and interpretation were carried out by R.H. The article was first drafted by R.H. and edited and revised by M.D.B. Final draft incorporating reviewer's comments was undertaken by R.H. and reviewed by M.D.B. All authors gave final approval for publication.

Competing interests. We have no competing interests.

Funding. The work was privately funded by R.H.

Acknowledgements. No other person voluntarily contributed to this research leading to the completion of this manuscript.

References

1. Shehata W, Lotfi H. 1993 Preconstruction solution for groundwater rise in sabkha. *Bull. Eng. Geol. Environ.* **47**, 145–150. (doi:10.1007/BF02639603)
2. Ioannou I, Hoff WD. 2008 Water repellent influence on salt crystallisation. *Proc. Inst. Civ. Eng. Constr. Mater.* **161**, 17–23. (doi:10.1680/coma.2008.161.1.17)
3. Culligan PJ, Ivanov V, Germaine JT. 2005 Sorptivity and liquid infiltration into dry soil. *Adv. Water Resour.* **28**, 1010–1020. (doi:10.1016/j.advwatres.2005.04.003)
4. Hall C, Hamilton A, Hoff WD, Viles HA, Eklund JA. 2011 Moisture dynamics in walls: response to micro-environment and climate change. *Proc. R. Soc. A* **467**, 194–211. (doi:10.1098/rspa.2010.0131)
5. Scherer GW. 2004 Stress from crystallization of salt. *Cem. Concr. Res.* **34**, 1615–1624. (doi:10.1016/j.cemconres.2003.12.034)
6. Le D, Hoang H, Mahadevan J. 2009 Impact of capillary driven liquid films on salt crystallisation. *Transport Porous Med.* **80**, 229–252. (doi:10.1007/s11242-009-9353-x)
7. Washburn ER. 1926 The creeping of solutions. *J. Phys. Chem.* **31**, 1246–1248. (doi:10.1021/j150278a009)
8. Hazlehurst TH, Martin HC, Brewer L. 1935 The creeping of saturated salt solutions. *J. Phys. Chem.* **40**, 439–452. (doi:10.1021/j150373a003)
9. Desarnaud J, Shahidzadeh-Bonn N. 2011 Salt crystal purification by deliquescence/crystallisation cycling. *Europhys. Lett.* **95**, 48002. (doi:10.1209/0295-5075/95/48002)
10. Dopfer D, Palzer S, Heinrich S, Fries L, Antonyuk S, Haider C, Salman AD. 2013 Adhesion mechanisms between water soluble particles. *Powder Technol.* **238**, 35–49. (doi:10.1016/j.powtec.2012.06.029)

11. Hird R, Bolton MD. 2014 Upward migration of sodium chloride by crystallisation on non-porous surfaces. *Philos. Mag.* **94**, 78–91. (doi:10.1080/14786435.2013.843794)
12. Sghaier N, Prat M. 2009 Effect of efflorescence formation on drying kinetics of porous media. *Transport Porous Med.* **80**, 441–451. (doi:10.1007/s11242-009-9373-6)
13. Veran-Tissoires S, Marcoux M, Prat M. 2012 Salt crystallisation at the surface of a heterogeneous porous medium. *Europhys. Lett.* **98**, 34005. (doi:10.1209/0295-5075/98/34005)
14. Sghaier N, Geoffroy S, Prat M, Eloukabi H, Ben Nasrallah S. 2014 Evaporation-driven growth of large crystallized salt structures in a porous medium. *Phys. Rev. E* **90**, 042402. (doi:10.1103/PhysRevE.90.042402)
15. Veran-Tissoires S, Prat M. 2014 Evaporation of a sodium chloride solution from a saturated porous medium with efflorescence formation. *J. Fluid. Mech.* **749**, 701–749. (doi:10.1017/jfm.2014.247)
16. Veran-Tissoires S, Marcoux M, Prat M. 2012 Discrete salt crystallisation at the surface of a porous medium. *Phys. Rev. Lett.* **108**, 054502. (doi:10.1103/PhysRevLett.108.054502)
17. Gran M, Carrera J, Massana J, Saaltink MW, Olivella S, Ayora C, Lloret A. 2011 Dynamics of water vapour flux and water separation processes during evaporation from a salty dry soil. *J. Hydrol.* (*Amst*). **396**, 215–220. (doi:10.1016/j.jhydrol.2010.11.011)
18. Rowe KR, Badv K. 1996 Advective-diffusive contaminant migration in unsaturated sand and gravel. *J. Geotech. Eng. ASCE* **122**, 965–975. (doi:10.1061/(ASCE)0733-9410(1996)122:12(965))
19. Richards LA. 1931 capillary conduction of liquids through porous mediums. *J Appl. Phys.* **1**, 318–333. (doi:10.1063/1.1745010)
20. Llewellyn PG. 1968 Dendritic halite pseudomorphs from the Keuper Marl of Leicestershire, England. *Sedimentology* **11**, 293–297. (doi:10.1111/j.1365-3091.1968.tb00858.x)
21. Southgate PN. 1982 Cambrian skeletal halite crystals and experimental analogues. *Sedimentology* **29**, 391–407. (doi:10.1111/j.1365-3091.1982.tb01802.x)
22. Castellazzi G, Colla C, de Miranda S, Formica G, Gabrielli E, Molari L, Ubertini F. 2013 A coupled multiphase model for hygrothermal analysis of masonry structures and prediction of stress induced by salt crystallisation. *Constr. Build. Mater.* **41**, 717–731. (doi:10.1016/j.conbuildmat.2012.12.045)
23. Shahidzadeh-Bonn N, Rafai S, Bonn D, Wegdam G. 2008 Salt crystallisation during evaporation: impact of interfacial properties. *Langmuir* **24**, 8599–8605. (doi:10.1021/la8005629)
24. Derluyn H *et al.* 2014 Characterising saline uptake and salt distributions in porous limestone with neutron radiography and X-ray micro-tomography. *J. Bldg. Phys.* **36**, 353–374. (doi:10.1177/1744259112473947)
25. Ruedrich J, Siegesmund S. 2007 Salt and ice crystallization in porous sandstones. *Environ. Geol.* **52**, 225–249. (doi:10.1007/s00254-006-0585-6)
26. Mullin JW. 2001 *Crystallisation*, 4th edn. Oxford, UK: Butterworth Heinemann.
27. Van Enckevort WJP, Los JH. 2013 On the creeping of saturated salt solutions. *Cryst. Growth Des.* **13**, 1838–1848. (doi:10.1021/cg301429g)
28. Sadeghi M, Taghikhani V, Ghotbi C. 2010 Measurement and correlation of surface tension for single aqueous electrolyte solutions. *Int. J. Thermophys.* **31**, 852–859. (doi:10.1007/s10765-010-0725-9)
29. Ozdemir O, Karakashev SI, Nguyen AV, Miller JD. 2009 Adsorption and surface tension analysis of concentrated alkali halide brine solutions. *Miner. Eng.* **22**, 263–271. (doi:10.1016/j.mineng.2008.08.001)
30. Sghaier N, Prat M, Nasrallah SB. 2006 On the influence of sodium chloride concentration on equilibrium contact angle. *Chem. Eng. J.* **122**, 47–53. (doi:10.1016/j.cej.2006.02.017)
31. Neumann AW. 1974 Contact angles and their temperature dependence: Thermodynamic status, measurement, interpretation and application. *Adv. Colloid Interface Sci.* **4**, 105–191. (doi:10.1016/0001-8686(74)85001-3)
32. Terzaghi K, Peck RB. 1964 *Soil mechanics in engineering practise*. New York, NY: Wiley.
33. Robinson DA, Jones SB, Wraith JM, Or D, Friedman SP. 2003 A review of advances in dielectric and electrical conductivity measurement in soils using time domain reflectometry. *Vadose Zone J.* **2**, 444–475. (doi:10.2136/vzj2003.4440)
34. Topp GC, Davis JL, Annan AP. 1980 Electromagnetic determination of soil water content: measurement in coaxial transmission lines. *Water Resour. Res.* **16**, 574–582. (doi:10.1029/WR016i003p00574)

35. Castiglione P, Shouse PJ. 2003 The effect of ohmic cable losses on time-domain reflectometry measurements of electrical conductivity. *Soil Sci. Soc. Am. J.* **67**, 414–424. (doi:10.2136/sssaj2003.4140)
36. Langlet M, Benali M, Pezron I, Saleh K, Guigon P, Metlas-Komunjer L. 2013 Caking of sodium chloride. Role of ambient relative humidity in dissolution and recrystallization process. *Chem. Eng. Sci.* **86**, 78–86. (doi:10.1016/j.ces.2012.05.014)
37. Gao Y, Chen SB, Yu LE. 2007 Efflorescence relative humidity of airborne sodium chloride particles: a theoretical investigation. *Atmos. Environ.* **41**, 2019–2023. (doi:10.1016/j.atmosenv.2006.12.014)
38. Langer JS. 1980 Instabilities and pattern formation in crystal growth. *Rev. Mod. Phys.* **52**, 1–30. (doi:10.1103/RevModPhys.52.1)
39. Du R, Stone HA. 1996 Evaporatively controlled growth of salt trees. *Phys. Rev. E* **53**, 994–997. (doi:10.1103/PhysRevE.53.1994)